

## Research Article

**Cite this article:** Umamaheswara Raju RS, Kottala RK, Madhava Varma B, Krishna P and Barmavatu P (2024). Internet of Things and hybrid models-based interpretation systems for surface roughness estimation. *Artificial Intelligence for Engineering Design, Analysis and Manufacturing*, **38**, e11, 1–19  
<https://doi.org/10.1017/S0890060424000192>

Received: 10 January 2024  
Revised: 24 May 2024  
Accepted: 09 June 2024


### Keywords:

cutting parameters; vibrations; sound characteristics; hybrid neural network model; Internet of things

### Corresponding author:

R. S. Umamaheswara Raju;  
Email: [mareshraju@mvgrce.edu.in](mailto:mareshraju@mvgrce.edu.in)

# Internet of Things and hybrid models-based interpretation systems for surface roughness estimation

R. S. Umamaheswara Raju<sup>1</sup> , Ravi Kumar Kottala<sup>1</sup>, B. Madhava Varma<sup>1</sup>,  
Palla Krishna<sup>1</sup> and Praveen Barmavatu<sup>2</sup>

<sup>1</sup>Department of Mechanical Engineering, M V G R College of Engineering (A), Chitalavalasa, Vizianagaram, Andhra Pradesh, India and <sup>2</sup>Department of Mechanical Engineering, Faculty of Engineering, Metropolitan Technological University, Santiago, Chile

## Abstract

Face milling is performed on aluminum alloy A96061-T6 at diverse cutting parameters proposed by the design of experiments. Surface roughness is predicted by examining the effects of cutting parameters (CP), vibrations (Vib), and sound characteristics (SC). Sound characteristics based on surface roughness estimation determine the rarity of the work. In this study, a unique ANN-TLBO hybrid model (Artificial Neural Networks: Teaching Learning Based Algorithm) is created to predict the surface roughness from CP, Vib, and SC. To ascertain their correctness and efficacy in evaluating surface roughness, the performance of these models is evaluated. First off, the CP hybrid model demonstrated an amazing accuracy of 95.1%, demonstrating its capacity to offer trustworthy forecasts of surface roughness values. The Vib hybrid model, in addition, demonstrated a respectable accuracy of 85.4%. Although it was not as accurate as the CP model, it nevertheless showed promise in forecasting surface roughness. The SC-based hybrid model outperformed the other two models in terms of accuracy with a remarkable accuracy of 96.2%, making it the most trustworthy and efficient technique for assessing surface roughness in this investigation. An analysis of error percentages revealed the exceptional performance of SC-based Model-3, exhibiting an average error percentage of 3.77%. This outperformed Vib Model-2 (14.52%) and CP-based Model-1 (4.75%). The SC model is the best option, and given its outstanding accuracy, it may end up becoming the go-to technique for industrial applications needing accurate surface roughness measurement. The SC model's exceptional performance highlights the importance of optimization strategies in improving the prediction capacities of ANN-based models, leading to significant advancements in the field of surface roughness assessment and related fields. An IoT platform is developed to link the model's output with other systems. The system created eliminates the need for manual, physical surface roughness measurement and allows for the display of surface roughness data on the cloud and other platforms.

## Introduction

Machining operations are performed on materials to attain better dimensional accuracy and surface roughness. Surface roughness is a crucial factor in manufacturing operations that influences the product's quality. Several factors influence material surface roughness, like cutting parameters, vibrations, cutting forces, coolant used, tool wear, chip formation, cutting tools, etc. (Anagün et al., 2023; RS et al., 2020; Chebrolu et al., 2022). A stylus probe device is used to manually test the surface roughness of the machined components. The probe instrument causes visible scratches on the machined parts by physically moving them (Raju et al., 2017; Guleria et al., 2022). Several researchers proposed artificial intelligence models for the prediction of surface roughness using the parameters that influence surface roughness to do away with the manual method of measurement (Huang et al., 2023; Yücel et al., 2023). Machine learning algorithms have been utilized more frequently lately to forecast surface roughness in manufacturing processes (Buj-Corral et al., 2023; Bhowmick et al., 2023). In this work, a novel hybrid model is created by combining the Teaching Learning Based Algorithm–Artificial Neural Networks) to enhance their capabilities. The complex relationships between the input variables (CP, Vib, and SC) and the output variable (surface roughness) are developed using the ANN. To improve accuracy, the ANN model's parameters are optimized using the TLBO technique. The study involves collecting experimental data on cutting parameters, vibration, and sound characteristics for a range of machining operations, and measuring the corresponding surface roughness. The ANN–TLBO hybrid model is trained on the gathered experimental data, and the model's effectiveness is assessed. The work aims to provide insights into the development of accurate and efficient models for predicting surface roughness in manufacturing processes. To

obtain the necessary surface finish, the manufacturing process parameters can be optimized using the suggested ANN–TLBO hybrid model. A mobile app is developed to interface with the sound characteristics, predict the surface finish, and display the same similar to Mikolajczyk *et al.* (2018). The remaining sections of the paper are organized as follows: 1. Introduction, 2 Literature review, 3. Experimentation, 4. Optimization of neural network models, 5. Models interpretation 6. Results, 7. IoT interface, and 8. conclusions

## Literature review

To carefully highlight the nuances of surface roughness prediction in CNC machining, the literature study is divided into three sections. Investigating the complex link between surface quality and machining circumstances through the analysis of cutting parameter-based systems. Deep insights into the critical function of vibration signals in surface roughness prediction were obtained by investigating vibrations-based systems. Meanwhile, the analysis of systems based on sound characteristics provided insightful viewpoints on how to use sound measurements for accurate surface quality evaluation. This methodical tripartite approach guarantees an exhaustive investigation of current approaches, providing a strong basis upon which our study may innovate and contribute to the area.

### Review on cutting parameter-based systems

Mikolajczyk *et al.* (2020) This research investigates the effect of oblique cutting with sintered carbide edges at different cutting-edge angles ( $\lambda_s$ ) on the minimal uncut chip thickness during free-radial rotation. The findings show that  $h_{min}$  decreases as  $\lambda_s$  angle increases, which is consistent with theoretical formulas pertaining to the direction of chip flow. Emphasizing the importance of non-orthogonal cutting processes in research and practice, the paper tackles micro-cutting and abrasive wear difficulties and proposes new avenues for finishing machining. Abbas *et al.* (2019) proposed an algorithm using an ANN with the Edgeworth–Pareto method that will optimize the cutting parameter in CNC face-milling operations. Surface roughness,  $R_a$ , has been forecasted utilizing a 3-10-1 multi-layer perceptron artificial neural network (ANN MLP) subsequent to completing the face milling process. The process involved parameters within the following ranges: cutting speed ranging from 78 to 158 m/min, cutting depth ranging from 0.5 to 1.5 mm, and feed per tooth ranging from 0.013 to 0.075 mm/tooth, with a precision of  $\pm 5.78\%$ . In the investigation of milling grade-H steel, neural network models have revealed a beneficial impact of spindle speed ( $n$ ) and feed rate ( $v_f$ ), and a detrimental impact of the depth of cut ( $a_p$ ) on surface roughness. Notably, the significance attributed to spindle speed and feed rate was 25 times greater than that assigned to the depth of cut. A three-axis, vertical CNC milling machine is used to perform end-mill operations on Aluminum 6061 T6a workpiece. Tseng *et al.* (2016) used a spindle touch probe and a Renishaw TS27R tool setting probe to measure the surface roughness. The cutting parameters from the experiment are taken as input variables for the fuzzy logic (FL) model to predict the surface roughness. Given a set of inputs, such as cutting speed, feed rate, and other variables, an FL model with 63 built to predict the surface roughness. The predicted values of the surface roughness (SR) from the FL model are compared with the values measured

experimentally, and the Model predicted them with an accuracy of 95%. Ho *et al.* (2009) conducted the end milling operation with various input parameters, such as speed feed rate and depth of cut, and measured the corresponding surface roughness value. With the aid of experimental values, they developed a novel hybrid Taguchi-genetic learning-based adaptive neuro-fuzzy inference system (HTGLA-based ANFIS) algorithm to predict the surface roughness value. In all, there are 72 experiments, of which 48 are used to train the model and 24 to test it. The developed model demonstrates superior performance and achieved an average error percentage of 4.06%. Eser *et al.* (2021) developed an experimental model using ANN and RSM to predict surface roughness in milling AA6061 alloy with TiCN-coated carbide tools. They found that the depth of cut had the most significant impact on surface roughness (35.48%), followed by cutting speed (23.38%), and feed rate (16.74%). This study underscores the importance of optimizing cutting parameters for improved surface quality in milling operations. Kara *et al.* (2023) investigated the impact of cutting parameters and nose radius variation on milling 17-4 PH stainless steel. They found that using a 0.4 mm cutting nose radius resulted in lower cutting force, temperature, and tool wear (approximately 2.35%, 28.89%, and 1.18% lower, respectively) compared to a 0.8 mm nose radius. Moreover, increasing the nose radius improved surface quality by an average of 47.48%. These findings highlight the importance of optimizing cutting parameters for enhanced machining performance and surface finish in stainless steel milling. Mikolajczyk *et al.* (2014) explored the critical influence of the thickness of an irreversible cut layer on the cutting process in low thickness layers, with reference to the radius of the cutting-edge rounding. It highlights how important this impact is for turning, especially when feed values are less than 0.05mm/rev for lower cutting-edge radii, allowing for higher feed rates for bigger radii. The created program facilitates the analysis and visualization of this impact, which is useful for maximizing machining parameters and comprehending the subtleties of surface roughness in turning processes.

### Review on vibrations-based systems

In the earlier section, the researchers built the predictive models for determining the surface roughness values by making use of the cutting parameters. Some studies on vibration-based surface roughness estimation are as follows: Wu and Lei (2019) performed the milling operation on S45C steel material using a tungsten carbide cutter, and corresponding vibrations were measured in all directions (i.e., X, Y, and Z directions). The vibrational signals have been extracted using a sensor and analyzed using time and frequency domain analysis in all specified directions. A BP-ANN model is developed to predict the surface roughness from cutting parameters and acquired vibration signals. The Z-direction vibration signal had more impact on the surface roughness than the other two directions. They also developed the three models (i.e., model 1: considering the cutting parameters as input parameters, model 2: considering the vibration data as input parameters, and model 3: combining both cutting and vibrational data) for predicting the surface roughness values. From the results, they found that the first model's mean absolute percentage error (MAPE) of the BP-ANN model is 29%. In the second model, MAPE is 25% when vibration signals are given as input for the prediction of surface roughness value. In the third model, MAPE is 19% when vibrations and cutting parameters are given as input. It is noticed that the surface roughness predictions are enhanced by combining

the vibration signals and cutting parameters. Feng et al. (2020) conducted the ultrasonic vibration-assisted slot milling operation on Aluminum alloy 2A12 samples using a five-axis machining center approach. The surfaces of workpieces are measured six times by an optical interferometer. The surface roughness of the slot after feed rate directional ultrasonic vibration-assisted milling is analyzed through the analytical predictive model. The analytical prediction model is compared with experimental measurements. The average percentage error is 13.4% for the first group of experiments under a spindle speed of 5,000 rpm. The average percentage error is 25.7% under the feed rate per tooth of 4  $\mu\text{m}$ . The average percentage error is 17.3% for the second group of experiments when the vibration amplitude is 4  $\mu\text{m}$ . The average percentage error is 10.9% when the vibration amplitude is 7  $\mu\text{m}$ . The proposed model achieved high accuracy in all cases. Župerl and Čuš (2019) performed the dry turning operation on AISI 8620 steel samples. In this experiment, the vibration signals are measured with accelerometers placed close to the tool. The signals from the accelerometers are processed and logged via a data acquisition card (DSPT Siglab Model 20-42) and the vibrational information is extracted during the experimentation. Surface roughness prediction is based on singular spectrum analysis (SSA), a unique signal processing technology that analyses the vibrations of cutting tools. In all, there are 60 experiments, of which 40 are used to train the model and 20 to validate it. The SSA model predicted SR values are predicted with an average percentage error of 4.72%.

### Review of sound characteristics-based systems

In the earlier section, the researchers built the predictive models for determining the surface roughness values by making use of the vibrational information during the machining operation. However, there is not an extensive amount of research that is available now that attempts to predict the surface roughness values by making use of the sound characteristics that have been gathered during the experiment. Salgado et al. (2009) performed the machining operation on mild steel specimens and gathered the friction noise characteristics as well as the contact force. With the aid of this information, a correlation has been developed between the surface roughness and input parameters (i.e., friction noise characteristics and contact force). The amplitude of friction noise and the magnitude of contact force are utilized to train a back propagation neural network (BPNN) for future prediction of Surface roughness. The network consisted of one output node and four input nodes. About 300 data sets are generated after the contactor is rubbed on surfaces made of mild steel that is machined. Among all, 30% of the data set is used to test the network's performance, and 70% of the randomly selected data is used to train the network. The data obtained from the experiments demonstrate that the neural network could learn the pattern for future prediction of surface roughness. Singh et al. (2004) performed the end milling machining operation on 16MnCr5 steel specimens. A cutting experiment with variable milling depth is carried out for the feasibility test of the cloud-based machining platform for monitoring end-milling operations. The cutting experiment is carried out using the CNC machine. The developed cloud machining platform's computing resources are linked to the machine tool's intelligent sensor system to create the two-level cyber-physical machining system. The designed smart optical sensor system can collect and transmit in real time the values of the cutting chip sizes to the cloud level. Based on the established cutting chip size, a cloud application with an adaptive neural

inference system is used to model and predict surface roughness online. By adjusting the machining parameters and maintaining surface roughness constant, a novel application of cognitive corrective control action is used to regulate the cutting chip size based on the in-process predictions. Controlled  $R_a$  deviated only less than 10% from the desired surface roughness value.

Zhao et al. (2022) conducted the slot milling machining operation on AL7075 workpiece samples with the aid of a 5-axis CNC machine. A total of 50 experiments are designed and conducted, out of which 40 are selected as the training set and the remaining 10 as the test set. A novel self-learning surface roughness prediction model has been developed based on the Pigeon-Inspired Optimized Support Vector Machine (PIO-SVM). The influence of cutter posture and cutting force on surface roughness is analyzed. The average prediction error of the proposed model was only 8.69% at the initial moment. A surface roughness stabilization method combining the proposed prediction model and digital twin technology is proposed to make the whole machined surface meet the surface roughness technology requirements. The proposed method had a good influence on making the surface roughness of the workpieces stable and helped to improve the machined surface properties, machining efficiency, and manufacturing cost.

## Methodology of experimentation

### Experimental setup

Face milling operations are performed on  $110 \times 50 \times 9 \text{ mm}^3$  sized aluminum alloy A96061-T6 flats at diverse cutting parameters. A spectrometer chemical analysis is done on the workpieces to test the composition, and the hardness of the material is measured to justify the above-mentioned material. A conventional milling machine named BFW VF1 (spindle motor of 3 kW and feed rate motors of 0.75 kW) is used to perform the face milling operation. A face milling cutter of 50 mm diameter with four numbers of teeth is used for machining. The placement of vibration sensor and the sound sensor are shown in Figure 1. Sensors are placed close to the spindle to acquire the spindle vibration data and sound characteristics. The sensors are connected to the national instruments data acquisition system (DAC) as shown in Figure 1.

The vibration measurement device (i.e., PCB single axis accelerometer, model number: 352C03, sensitivity ( $\pm 20\%$ ): 9.95 mV/g, frequency range ( $\pm 5\%$ ): 0.5–10,000 Hz, measurement range:  $\pm 500 \text{ g Pk}$ , resonant frequency:  $\geq 50 \text{ kHz}$ , weight (without cable): 5.8g) is used for the measurement of vibrations and the overall vibration values. The obtained vibrational values are given in Table 1. The sound sensor or microphone with a sensitivity of 45 mV/Pa is used to measure the overall sound characteristics during the experimentation. The obtained sound characteristics are listed in Table 1. Specifications of the sound sensor are model number: 377B02, open circuit sensitivity: 45 mV/Pa, frequency range ( $\pm 2 \text{ dB}$ ): 3.15 Hz–20 kHz, dynamic range upper limit: 3%: 146 dB A. National instruments (NI) data acquisition (DAQ) systems, cDAQ-SV1101 Bundle specifically designed for vibration and sound measurements, are used in this experiment. This system is used to capture and analyze data from accelerometer and microphones to characterize vibrations and acoustic signals in the test section. The cDAQ-SV1101 Bundle is a one-slot chassis that can accommodate up to four signal conditioning modules (SCMs). Each SCM can support up to four channels of measurement, and the system can sample at up to



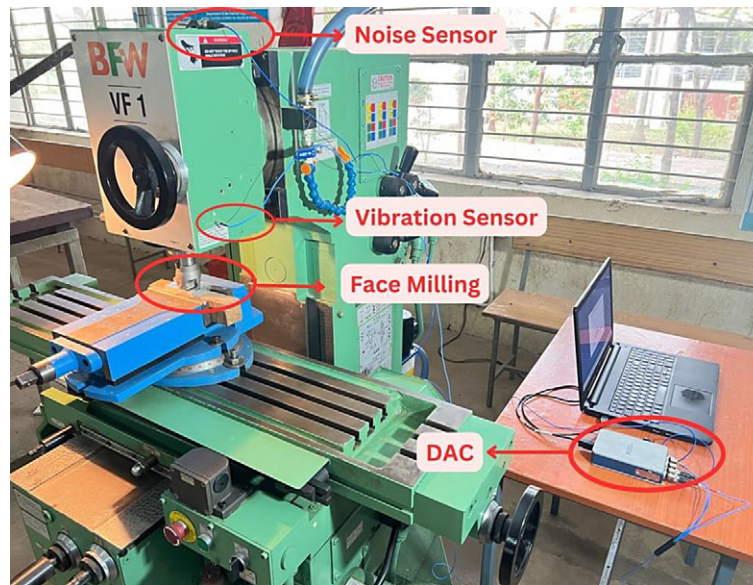


**Figure 1.** Vibration sensor and sound sensor connected to DAC for data acquisition.

**Table 1.** Plan of experiments and given results of overall vibrations ( $m/s^2$ ), overall sound (dB), and surface roughness ( $\mu m$ )

Experiment number	Speed (rpm)	Feed rate (mm/min)	D.O.C (mm)	Overall vibrations ( $m/s^2$ )	Overall sound (dB)	Surface roughness ( $\mu m$ )
1	1000	160	0.6	5.00	99.68	0.846
2	1400	160	0.4	4.45	92.65	1.071
3	710	160	0.2	3.37	90.36	1.417
4	1400	200	0.2	4.45	93.74	0.306
5	1400	160	0.2	5.02	98.20	0.535
6	710	200	0.2	3.49	95.01	2.280
7	1000	100	0.2	3.95	95.94	1.801
8	1400	100	0.6	4.98	98.47	0.5
9	1400	100	0.4	4.92	98.42	0.4
10	710	100	0.2	3.34	94.55	1.22
11	1400	160	0.6	4.33	97.06	0.549
12	710	160	0.4	4.19	96.59	1.45
13	1000	200	0.4	6.09	99.91	1.529
14	710	100	0.4	3.61	95.47	0.3658
15	1000	100	0.6	4.93	98.17	1.046
16	1000	160	0.2	4.48	97.25	0.498
17	1000	100	0.4	4.68	97.90	0.839
18	710	100	0.6	3.89	96.37	0.935
19	1400	200	0.6	6.42	100.51	0.815
20	1000	200	0.6	5.78	99.74	1.226
21	710	200	0.4	4.28	96.85	1.314
22	710	160	0.6	4.42	96.98	0.587
23	1000	160	0.4	5.12	98.77	1.86

(Continued)

**Table 1.** (Continued)

Experiment number	Speed (rpm)	Feed rate (mm/min)	D.O.C (mm)	Overall vibrations ( $m/s^2$ )	Overall sound (dB)	Surface roughness ( $\mu m$ )
24	1000	200	0.2	4.82	98.16	0.62
25	1400	100	0.2	4.85	97.81	0.552
26	710	200	0.6	4.69	97.35	1.23
27	1400	200	0.4	5.65	99.20	0.896

51.2 kS/s per channel with 24-bit resolution. In the design of experiments (DOE), a methodical approach is used to set the experimental cutting parameters required for machining in a sequential order. The cutting parameters given for DOE (Design Expert V13 software) are cutting speed (i.e., 710, 1000, and 1400 rpm), feed rate (i.e., 100, 160, 200 mm/min), and depth of cut (D.O.C.) (i.e., 0.2, 0.4, and 0.6 mm) and a total of 27 different experiments are proposed by DOE for experimentation, as listed in Table 1. The Talysurf is used to measure the surface roughness of each machined flat, and the measured surface roughness values to its corresponding cutting parameters are shown in Table 1.

### Experimental results

Three alternative ANN–TLBO hybrid models are created using the experimental data from Table 1. Model 1 is created to map the cutting parameters and surface roughness, while model-2 and model-3 are created to map overall vibrations and sound characteristics to predict surface roughness, respectively. The model-2 and model-3 contained single data, as shown in Table 1, which resulted in model prediction errors as high as 25%. To solve the aforementioned issue, the maximum amplitudes at associated frequencies are documented and displayed in Table 2 for each experimental vibration data set. The graphs between the amplitude and frequency of many tests are superimposed. To plot the

**Table 2.** Vibrations amplitudes and surface roughness values

Exp. No	AMP-1	AMP-2	AMP-3	AMP-4	AMP-5	AMP-6	Measured surface roughness (μm)	Predicated surface roughness (μm)	Error (%)
1	0.112	0.621	0.243	0.724	2.094	0.188	0.846	0.789	6.738
2	0.153	0.156	0.638	0.372	0.357	0.125	1.071	0.942	12.045
3	0.617	0.098	0.507	0.245	0.268	0.078	1.417	1.045	26.253
4	0.096	0.105	1.386	0.313	0.320	0.135	0.306	0.378	23.529
5	0.113	0.122	0.334	0.295	0.302	0.134	0.535	0.456	14.766
6	0.694	0.098	0.461	0.368	0.292	0.079	2.280	2.010	11.842
7	0.093	0.380	0.180	0.502	1.397	0.186	1.801	1.601	11.105
8	0.132	0.128	0.538	0.397	0.370	0.132	0.500	0.412	17.600
9	0.127	0.517	0.222	0.614	0.866	0.210	0.400	0.421	5.250
10	0.429	0.052	0.458	0.297	0.253	0.063	1.064	0.987	7.237
11	0.116	0.121	0.565	0.373	0.406	0.146	0.549	0.478	12.933
12	0.858	0.139	0.467	0.387	0.360	0.088	1.450	1.324	8.690
13	0.137	0.696	0.218	0.461	2.053	0.210	1.529	1.124	26.488
14	0.553	0.061	0.417	0.367	0.281	0.071	0.366	0.246	32.859
15	0.118	0.539	0.287	0.438	1.527	0.201	1.046	0.945	9.656
16	0.097	0.412	0.254	1.464	0.723	0.191	0.498	0.589	18.273
17	0.094	0.376	0.199	0.781	1.466	0.185	0.839	0.912	8.701
18	0.696	0.068	0.372	0.326	0.302	0.073	0.935	0.789	15.615
19	0.151	0.165	2.139	0.618	0.387	0.184	0.815	0.745	8.589
20	0.131	0.839	0.298	0.982	1.979	0.130	1.226	1.045	14.763
21	0.982	0.102	0.381	0.330	0.344	0.099	1.314	1.541	17.276
22	0.698	0.088	0.498	0.438	0.277	0.091	0.587	0.498	15.162
23	0.127	0.552	0.235	1.303	0.890	0.149	1.860	1.612	10.444
24	0.094	0.098	0.264	0.516	0.332	0.121	0.620	0.512	17.419
25	0.107	0.109	0.406	0.382	0.382	0.121	0.552	0.589	6.703
26	0.918	0.096	0.553	0.412	0.312	0.095	1.230	0.986	19.837
27	0.152	0.152	1.995	0.514	0.375	0.144	0.896	0.786	12.277

Average error = 14.520.  
 RMSE = 0.154.  
 R<sup>2</sup> = 0.885.

graphs, the pattern has been followed, as it can involve maintaining the first two cutting parameters constant and changing the third parameter. After evaluating the results, it is noticed that the greater amplitude peaks are observed at frequencies of 411.648, 828.416, and 1644.584 Hz with increasing speed. Similar amplitude peaks are observed at different frequencies 411.648, 601.089, and 1202.176 Hz at varied feed rate, and amplitude peaks are observed at different frequencies at varied depth of cut is 411.648, 828.416, and 1149.95 Hz, respectively. The largest amplitudes and their related frequencies are tabulated, and the data is utilized to develop the hybrid model-2.

The hybrid model-3 is developed using the mean, standard deviation, skewness, and kurtosis values that are calculated for each experiments sound characteristics and are shown in Table 3. The following Eqs. (1)–(4) are used to calculate average values of sound characteristics used for prediction of surface roughness.

$$Mean = \sum \frac{\bar{X}}{N} \tag{1}$$

where  $\bar{X}$  is the sum of all the values, and  $N$  is the number of values in the sample.

$$Standard\ Deviation(\sigma) = \sqrt{\frac{1}{N-1} \sum_{i=1}^N (x_i - \bar{x})^2} \tag{2}$$

where  $x_i$  is each value in the sample,  $\bar{x}$  is the sample mean, and  $N$  is the number of values in the sample.

$$Skewness = \left[ \frac{n}{(n-1)(n-2)} \right] \times \sum \left[ \frac{x_i - \bar{x}}{\sigma} \right]^3 \tag{3}$$

where  $n$  is the sample size,  $x_i$  is the  $i$ th observation in the dataset,  $\bar{x}$  is the sample mean and  $\sigma$  is the sample standard deviation.

**Table 3.** Sound characteristics and surface roughness values

Exp. no.	Mean	Standard deviation	Skewness	Kurtosis	Measured surface roughness ( $\mu\text{m}$ )	Predicted surface roughness ( $\mu\text{m}$ )	Error (%)
1	0.008	0.246	-0.039	1.013	0.846	0.799	5.615
2	0.007	1.057	0.008	1.390	1.071	1.117	4.314
3	-0.005	0.742	-0.091	0.915	1.417	1.446	2.040
4	0.021	0.880	0.163	2.971	0.306	0.296	3.366
5	-0.006	1.639	0.006	2.239	0.535	0.507	5.196
6	-0.003	1.283	-0.021	0.749	2.280	2.271	0.395
7	0.012	1.514	-0.109	1.371	1.801	1.727	4.131
8	0.014	1.900	0.008	1.064	0.500	0.528	5.680
9	0.012	1.660	0.026	1.301	0.400	0.401	0.175
10	-0.004	1.107	-0.055	1.703	1.064	1.109	4.248
11	0.005	2.069	-0.044	2.121	0.549	0.549	0.073
12	-0.001	1.422	0.072	1.073	1.450	1.420	2.076
13	0.005	2.091	-0.060	0.661	1.529	1.462	4.382
14	-0.008	1.261	-0.013	0.996	0.366	0.336	8.201
15	0.001	1.812	-0.101	1.363	1.046	1.020	2.199
16	-0.011	1.742	-0.095	2.117	0.498	0.466	6.337
17	-0.021	1.739	0.012	2.112	0.839	0.902	7.557
18	0.012	1.399	-0.014	0.611	0.935	0.940	0.481
19	0.008	2.301	0.006	1.448	0.815	0.819	0.442
20	-0.008	2.190	-0.121	0.372	1.226	1.181	3.703
21	0.004	1.543	0.041	0.450	1.314	1.338	1.819
22	-0.004	1.530	0.043	0.418	0.587	0.618	5.332
23	0.005	1.834	-0.017	1.035	1.860	1.733	3.750
24	-0.030	1.818	-0.034	1.548	0.620	0.586	5.565
25	0.007	1.569	-0.027	1.616	0.552	0.525	4.909
26	-0.001	1.613	-0.079	0.538	1.230	1.254	1.976
27	0.000	2.066	-0.008	1.498	0.896	0.965	7.746

Average error = 3.781 %.

RMSE = 0.048.

 $R^2 = 0.988$ .

$$\text{Kurtosis} = \frac{(n \times (n + 1))}{(n - 1)(n - 2)(n - 3)} \times \left( \sum \left[ \left( \frac{(x_i - \bar{x})^4}{\sigma^4} \right) \right] \right) - \frac{[(n - 1)^2]}{[(n - 2)(n - 3)]} \quad (4)$$

where  $n$  is the sample size,  $x_i$  is the  $i$ th observation in the dataset,  $\bar{x}$  is the sample mean, and  $\sigma$  is the sample standard deviation.

## Optimization of neural network models

### Artificial neural network (ANN)

An artificial neural network is a simplified nonlinear computational and mathematical model that is able to solve many engineering problems, including modeling, and prediction of experimental values Kottala *et al.* (2022). Nowadays, neural networks have become the most popular technique to predict experimental outcomes and show

comparatively better performance than the existing traditional methods. The ANN structure consists of an input layer, an output layer, and hidden layers. The number of neurons present in the input layer and output layer is equal to the number of considered input and output parameters, respectively. Typically, a neural network contains processing elements connected via weighted interconnections. Each processing element receives input signals via weighted incoming connections Kumar *et al.* (2022). Mikolajczyk and Olaru (2015) performed regression analysis for practical modeling is presented in the paper, along with its uses and drawbacks. Regression analysis offers a good mathematical model, but choosing the right model requires a thorough understanding of the phenomena. The relative error can be used to measure the correctness of a model, as neural networks provide a large adjustment range but lack information on model coefficients or factor importance. Neural network extrapolation proved to be a powerful tool for assessing quality beyond experimental data, and this capacity was investigated further. Kara

et al. (2020) studied cutting parameter effects on surface roughness and tool wear in AISI D2 cold work tool steel with different heat treatments using ceramic cutting tools. They employed an ANN model for surface roughness prediction, achieving high accuracy ( $R^2 > 0.97$ ,  $RMSE < 0.07$ ). The study highlights the influence of deep cryogenic processing on material hardness and demonstrates the ANN's strong learning capacity for surface roughness estimation.

A suitable learning method was adopted to train the network structure by changing the weights and bias of every neuron. The training process continues until it reaches the lowest root mean square error (MSE). By varying the weights and biases of the network will reduce the error between the predicted and desired values. The following Eq. (5) is effectively utilized to create the network structure.

$$F(H_n) = \frac{2}{1 + e^{-2 \times \left( \sum_{j=0}^n (W_{ij} \times X_i) + b_j \right)}} - 1 \quad (5)$$

Present ANN structure, the input neuron receives the total information from the input data i.e.,  $X_i$ . Equation (5)  $W_{ij}$  represents the connection weight from the input layer to the hidden layer and  $b_j$  is the bias of each hidden neuron. Whereas  $W_{jk}$  and  $b_k$  denotes weight connections between the hidden layer and output layer and bias respectively.

$$O_k = \sum_{k=0}^n (W_{jk} \times H_n) + b_k \quad (6)$$

The predicted output of each output neuron ( $O_k$ ) can be calculated by using the above Eq. (6). The Tansig activation function is chosen between the input and hidden layer whereas the Purelin activation functions is used for the output layer. The number of neurons present in the hidden layer plays a vital role in the predictability of the network. If too few neurons in the hidden layer may lead to less precise outcomes, too many neurons will not give fair results. So, it is required to optimize the number of neurons in the hidden layer. The number of neurons can be determined by using the trial-and-error method. The optimum neurons are calculated by using the following Eq. (7) (Balasubramanian et al., 2022). The learning rate function in this hybrid neural network is regarded as fixed and has a value of 0.001. Freed forward neural networks that are optimized with the aid of the TLBO algorithm eliminate the sensitivity analysis of the learning rate function. Independent of learning rate function, TLBO optimizes the weights and bias [19, 21].

$$H_n = \frac{\text{Input} + \text{Output}}{2} + \sqrt{\text{Train data}} \quad (7)$$

To improve the accuracy of outcomes, it is necessary to normalize the input data (cutting parameters). This normalization can be used to improve the accuracy as well as reduce the convergence time. The input and output data are normalized within the range of 0–1 for cutting parameter as data is diverse. The data normalization can be calculated using the following Eq. (8) (Kottala et al., 2023).

$$X = \frac{(X_i - X_{\min})}{(X_{\max} - X_{\min})} (\text{high}_{\text{value}} - \text{Low}_{\text{value}}) + \text{Low}_{\text{value}} \quad (8)$$

### Teaching learning-based optimization (TLBO) algorithm

Teaching learning-based optimization (TLBO) is the most popular meta-heuristic approach in recent years and was proposed by Rao

et al. (2012). Compared to other stochastic searching algorithms, TLBO has advantages like higher accuracy, simplicity in structure, and quicker convergence. TLBO mainly comprises two parts, i.e., the teacher phase and the learner phase. In this algorithm, the 'Teacher phase' mode means learning from the teacher, whereas the 'learner phase' means learning from communication between the learners. The teacher phase and learner phase are well described in the below sub-sections Teacher phase and Student/learner phase.

### Teacher phase

The teacher phase is the preliminary stage of the TLBO algorithm where the teacher shares knowledge with the students based on the normal distribution function as mentioned in Eq. (9) below and the schematic representation of the TLBO is shown in Figure 2.

$$f(X) = \frac{1}{\sigma\sqrt{2\pi}} \times e^{\left\{ \frac{-(x-\mu)}{\sigma^2} \right\}} \quad (9)$$

where  $\sigma^2$ ,  $\mu$  represents the variance and mean of the sample function, respectively.

The students gained knowledge from the teacher and enhanced their average knowledge level by interacting with the teacher. In the teacher phase, for a specified initial population, calculate the objective function value. After that, evaluate the mean value of all individuals, the best solution is achieved. If the best solution is better than the previous one, then it is stored as the best solution. The new solution can be determined by the following Eq. (10).

$$X_{\text{new}} = X_{\text{older}} + r(X_{\text{teacher}} - T_f \times \text{mean}) \quad (10)$$

where 'r' is denoted as random number and range of selection of 0–1,  $X_{\text{Teacher}}$  means obtained results from the teacher,  $T_f$  is the teaching factor which is randomly taken from 1 to 2.

$$T_f = \text{round}(1 + \text{rad}(0.1)(2 - 1)) \quad (11)$$

The teaching factor ( $T_f$ ) value cannot be set by the user and this parameter determined by the algorithm using the above Eq. (11).

### Student/learner phase

In the learner phase, the learner's knowledge is increased by two processes: initially, by the teacher's input and next, by interaction among the neighborhood learners. These learners communicate with each other and upgrade their knowledge with the help of discussions between themselves. Whoever has more knowledgeable student will transfer knowledge to the less knowledgeable student. After certain iterations, the all less knowledgeable students gained more knowledge interacting with them. As a result, the final outcome of the generated population is better than the initial population. The following Eq. (12) is used to evaluate the performance of the learner by means of its fitness value.

$$X_{\text{new},i} = \begin{cases} X_{\text{old}+r}(X_i - X_j) & \text{if } f(X_i) < f(X_j) \\ X_{\text{old}+r}(X_j - X_i) & \text{Else where} \end{cases} \quad (12)$$

where  $X_i$ ,  $X_j$  are the randomly selected individuals in the learner phase,  $X_{\text{new},i}$  is the new solution after the learner phase and 'r' denotes random number between 0 and 1.

### ANN-TLBO

Integration of the TLBO algorithm to neural network was suggested for current research work, in order to overcome the limitations of conventional ANN architecture. The major reason for implementing



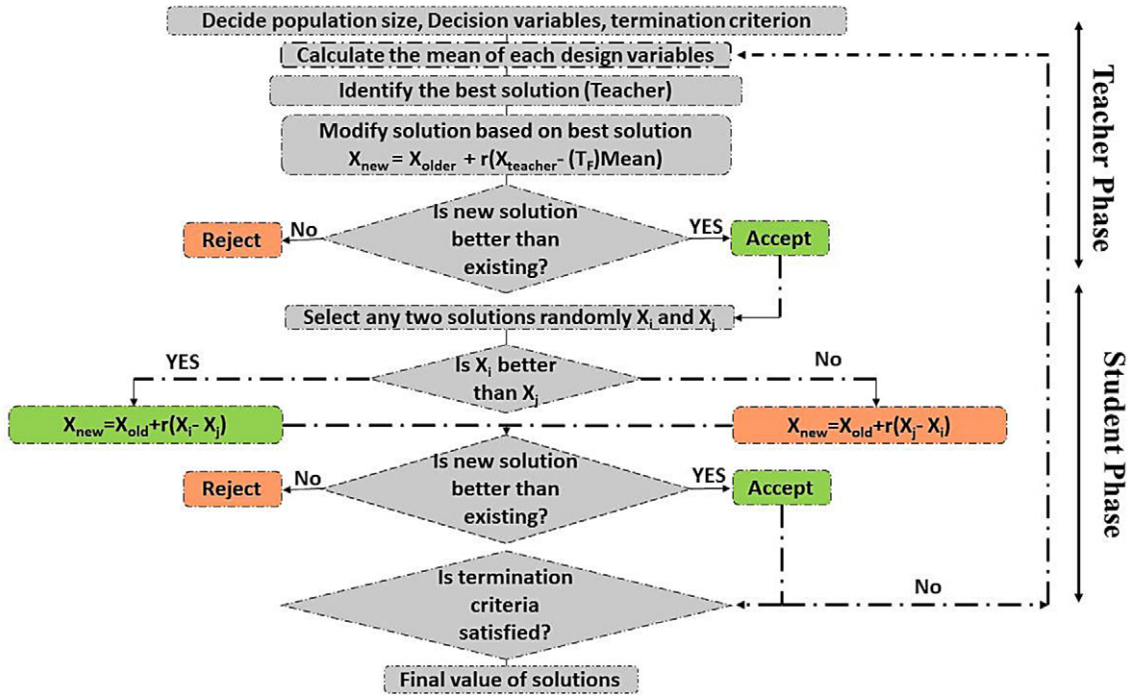


Figure 2. Schematic representation of the teacher-learner-based algorithm.

the TLBO algorithm to ANN was able to determine the optimal solution with minimum computational cost. This hybrid TLBO-ANN is used to train the experimental dataset, to achieve the optimal solutions for the weights and biases, which can be used to reduce the MSE in a short span of period. These selected parameters are progressively updated until they reaches the convergence criterion. The main objective function of the TLBO is to minimize the MSE. The working of the proposed hybrid algorithm is shown in Figure 3. The following Eqs. (13) and (14) are used to evaluate the

performance of the hybrid ANN-TLBO algorithm. In the TLBO algorithm, there are mainly two parameters population size; and the number of iterations will decide the accuracy of the algorithm. Using a trial-and-error approach, these control parameters are set to fixed until they obtain the lowest MSE.

$$RMSE = \sqrt{\frac{1}{n} \sum_{i=1}^n (X_A - X_P)^2} \tag{13}$$

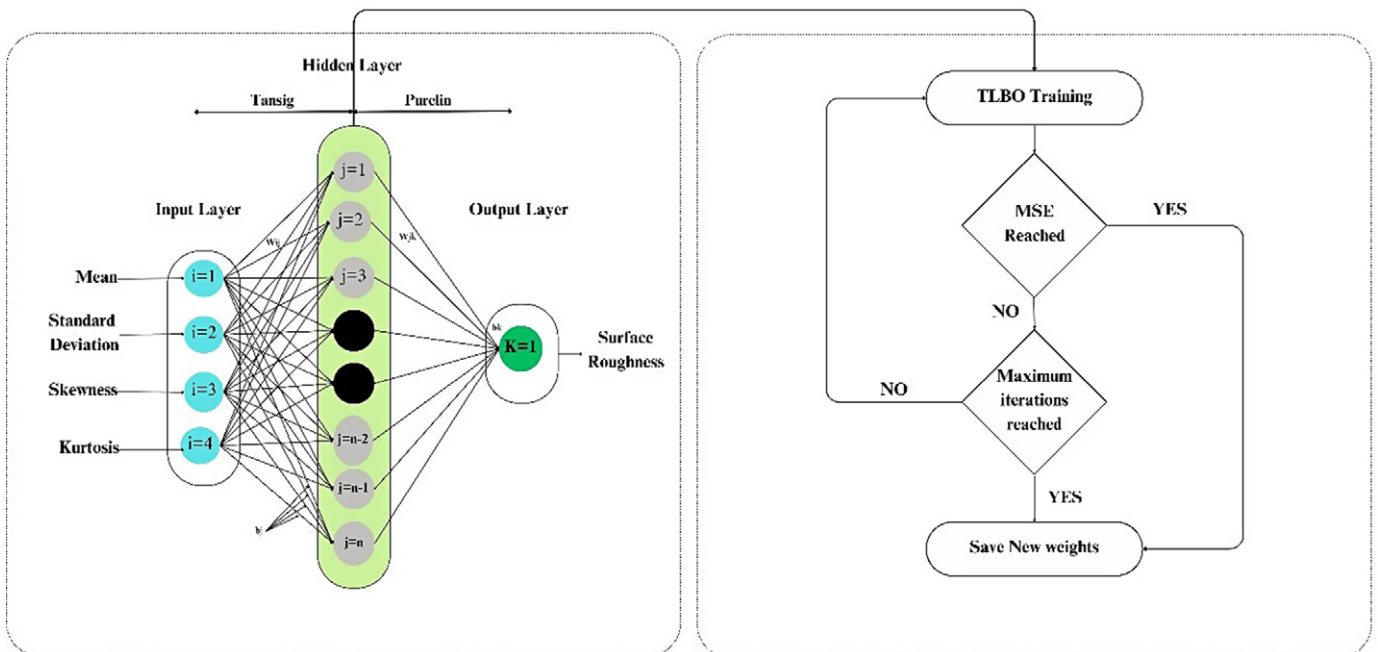


Figure 3. Schematic representation of working of ANN-TLBO hybrid model.



$$R^2 = 1 - \frac{\sum (X_i - X_p)^2}{\sum (X_i - \bar{X}_i)^2} \tag{14}$$

**Models Interpretation**

*Cutting parameters based hybrid model*

Due to the numerous intricate interactions between the cutting parameters, the connection between cutting parameters and surface roughness is not always linear. To overcome the non-linearity, an ANN-TLBO hybrid model is developed to predict surface roughness. The hybrid model consists of three parameters, namely the number of hidden neurons ( $H_o$ ), population size ( $n_{pop}$ ), and maximum iterations (Max It), that need to be determined to achieve the best predictions. The number of hidden neurons is calculated based on Eq. (7) and tested with a variance of  $\pm 5$  of the optimal hidden neurons. The hybrid model is trained and tested by keeping the number of hidden neurons (ranging from 2, 3, 4.....12) constant, correspondingly varying the population size (ranging from 25, 50, 75..... 275) and maximum iterations (ranging from 100, 200, 300.....1100). The MSE is calculated for each neuron in order to determine the optimal number of hidden neurons. The number of hidden neurons with the lowest MSE is considered the optimal number of neurons for the hybrid model. After finding the optimal hidden neuron, population size is kept constant by varying the number of hidden neurons and maximum iterations, respectively. Similarly, the above procedure is repeated by keeping the maximum number of iterations (Max It) constant. The results of optimal hidden neuron ( $H_o = 6$ ), population size ( $n_{pop} = 125$ ), and Max It = 700. As the algorithm continues its iterations, it endeavors to enhance the solution by adjusting the candidate solutions in the population. As time progresses, the cost (or fitness) function value tends to decrease in a gradual manner. Consequently, there is an overall downward trend in the optimal cost as iterations proceed.

This study followed a meticulously approach called the “Leave-One-Out Cross-Validation” (LOOCV) method of optimization. In LOOCV, the dataset is repeatedly divided into a training set that contains all data points except one and a test set that only contains that one missing data point (Kundu et al. 2022, Horñas et al, 2023). To evaluate the model’s performance more than once, this procedure is repeated for each data point in the dataset. The outcomes are then averaged or otherwise compiled to determine the model’s overall performance. LOOCV is often used to assess the predictive power and generalization ability of machine learning models when the dataset is limited. The above method is provided in [supplementary data file](#).

The scatter plot is drawn between predicted and measured roughness over the number of experiments and is shown in Figure 4. The variation between the predicted and measured roughness is shown graphically. There is a significant correlation between the predicted and measured roughness. If the data points are close to each other and form a tight cluster, it indicates that there is a strong relationship, whereas if the data points are widely dispersed, it suggests that there is little correlation between the two variables.

The RMSE and  $R^2$  are used to evaluate the performance of the model, as shown in Figure 5. The line diagram shows the relationship between the neurons with their corresponding RMSE and  $R^2$ . This shows that neuron 6 is the most accurate and precise neuron, with the lowest RMSE value of 0.068 and the highest  $R^2$  value of 0.993 compared to other neurons. The low RMSE indicates that predicted values are close to the actual values, while the high  $R^2$  value indicates that the model explains a large portion of the variance in the data. The empirical formulas for calculating RMSE and  $R^2$  are given in Eqs. (13) and (14), respectively.

The above graph shown in Figure 6 indicates the neuron 6 curve has the lowest percentage error when compared to other neurons. This indicates that neuron 6 is the optimal neuron among all the neurons tested. The graph indicates optimal hidden neurons as ( $H_o=6$ ), population size ( $n_{pop} = 125$ ), and Max It = 700. The RMSE, correlation coefficient ( $R^2$ ), and MEP

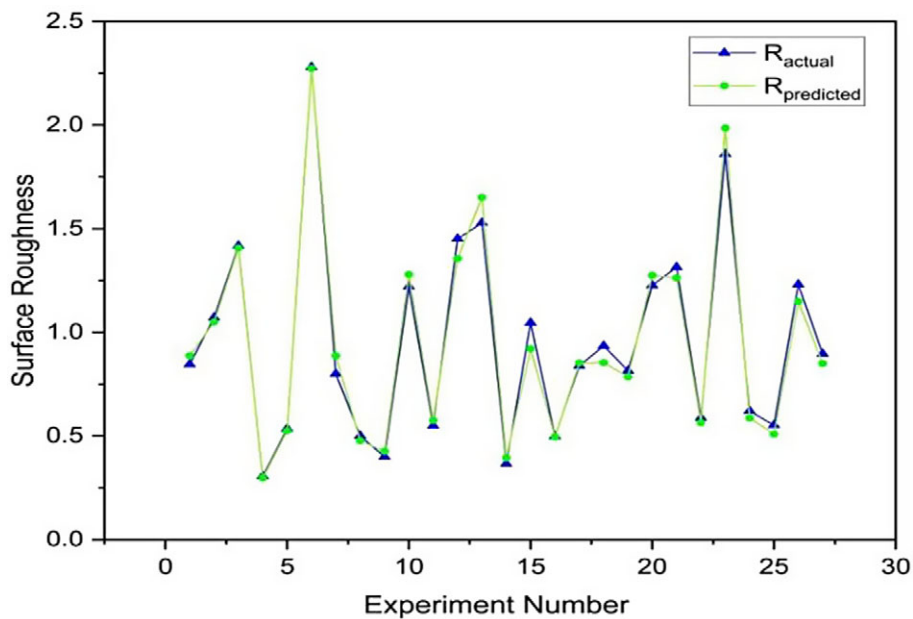


**Figure 4.** Measured surface roughness ( $R_{actual}$ ) vs Predicted surface roughness ( $R_{predicted}$ ) for model 1.

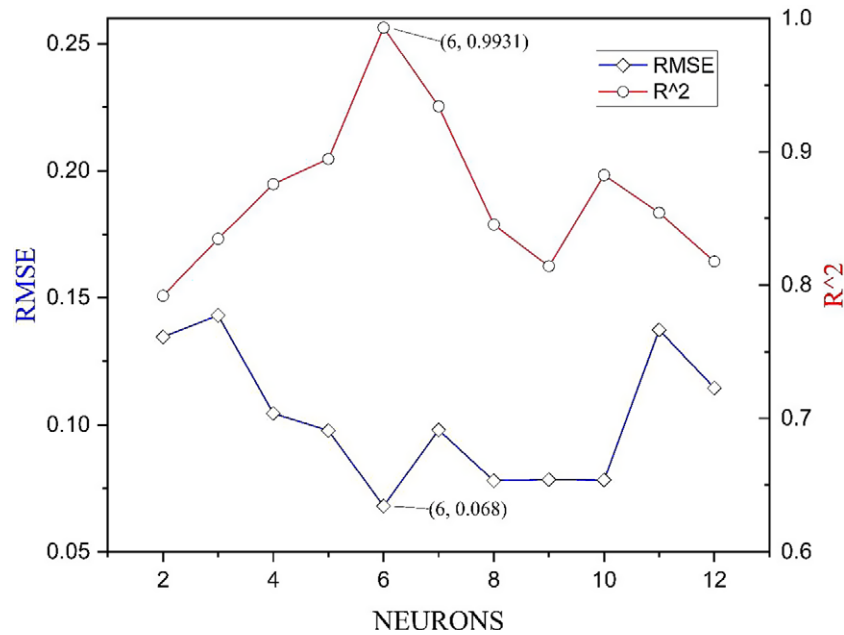


Figure 5 Calculated RMSE and  $R^2$  values at each hidden neuron for model 1.

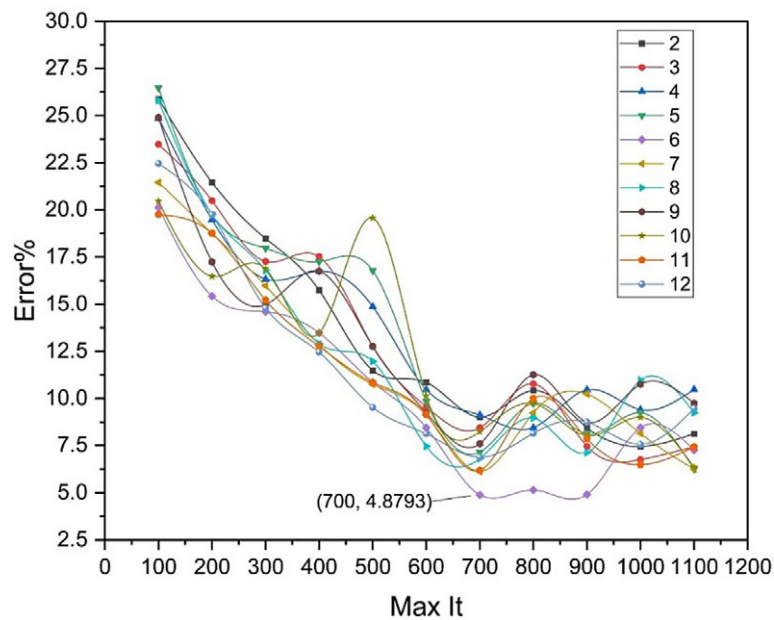


Figure 6 Calculated error percentage at each maximum iteration and each hidden neuron for model 1.

values obtained with these algorithms for model-1 are shown in Tables 4 and 5.

**Vibrations-based hybrid model**

As mentioned earlier in experimentation, the overall vibration data is used for the vibration-based hybrid model development, and the model prediction error percentage is high. The graphs are drawn and superimposed between amplitude and frequency by maintaining the first two cutting parameters constant and changing the third. After evaluating the graphs, it is possible to conclude that the greater amplitude peaks are observed at frequencies 411.648,

601.089, 828.416, 1149.95, and 1644.584 Hz. The frequencies and their related amplitudes are tabulated in Table 2, and the data is utilized to develop the hybrid model 2. AMP-1 in Table 2 indicates the amplitude of vibration at a frequency of 411.648 Hz; similarly, AMP-2 indicates the amplitude of vibration at a frequency of 601.089 Hz, and so on.

The scatter plot is drawn between predicted and measured roughness over the number of experiments and is shown in Figure 7. The variation between the predicted and measured roughness is shown graphically. There is a significant correlation between the predicted and measured roughness. If the data points are close to each other and form a tight cluster, it indicates that

**Table 4.** Model-1 RMSE and  $R^2$  values for different neurons generated by the algorithm

Neuron	RMSE	$R^2$
2	0.134	0.792
3	0.143	0.834
4	0.104	0.875
5	0.097	0.894
6	0.068	0.993
7	0.098	0.934
8	0.078	0.845
9	0.078	0.814
10	0.078	0.882
11	0.137	0.854
12	0.114	0.817

there is a strong relationship, whereas if the data points are widely dispersed, it suggests that there is little correlation between the two variables.

The RMSE and  $R^2$  are used to evaluate the performance of the model as shown in Figure 8. The line diagram shows the relationship between the neurons with corresponding RMSE and  $R^2$ . This shows that neuron 10 is the most accurate and precise neuron with the lowest RMSE value of 0.154 and the highest  $R^2$  value of 0.885 compared to other neurons. The low RMSE indicates that predicted values are close to the actual values, while its high  $R^2$  value indicates that the model explains a large portion of the variance in the data.

The below graph shown in Figure 9 indicates the neuron 10 curve has the lowest %error when compared to other neurons. This indicate that the neuron 10 is the optimal neuron among all the neurons tested. The graph indicates optimal hidden neuron as ( $H_o = 10$ ), population size ( $n_{pop} = 200$ ), and Max It = 800. The RMSE, correlation coefficient ( $R^2$ ), and MEP values obtained with these algorithms are shown in Tables 6 and 7.

**Table 5.** Model-1 MEP values for different neurons generated by the algorithm

Max It	2	3	4	5	6	7	8	9	10	11	12
100	25.874	23.47	24.862	26.457	20.12	21.457	25.789	24.897	20.45	19.745	22.46
200	21.458	20.475	19.475	19.741	15.428	18.745	19.745	17.235	16.478	18.745	19.745
300	18.475	17.263	16.326	17.965	14.589	15.975	16.785	14.978	16.874	15.213	14.785
400	15.745	17.52	16.751	17.256	13.475	12.864	12.892	16.745	13.457	12.756	12.453
500	11.476	12.745	14.875	16.782	10.856	10.745	11.963	12.756	19.562	10.852	9.523
600	10.856	9.562	10.475	9.845	8.452	9.123	7.456	9.245	10.142	9.142	8.125
700	9.012	8.456	9.12	7.142	4.879	6.127	6.814	7.587	8.235	6.178	6.874
800	10.425	10.782	8.452	9.745	5.142	9.235	8.963	11.251	9.745	10.004	8.147
900	8.456	7.452	10.457	8.124	4.901	10.235	7.125	8.745	8.014	7.852	8.745
1000	7.452	6.745	9.412	9.243	8.452	8.145	10.963	10.76	9.004	6.475	7.547
1100	8.124	7.425	10.475	6.245	7.256	6.254	9.245	9.745	6.347	7.415	9.475

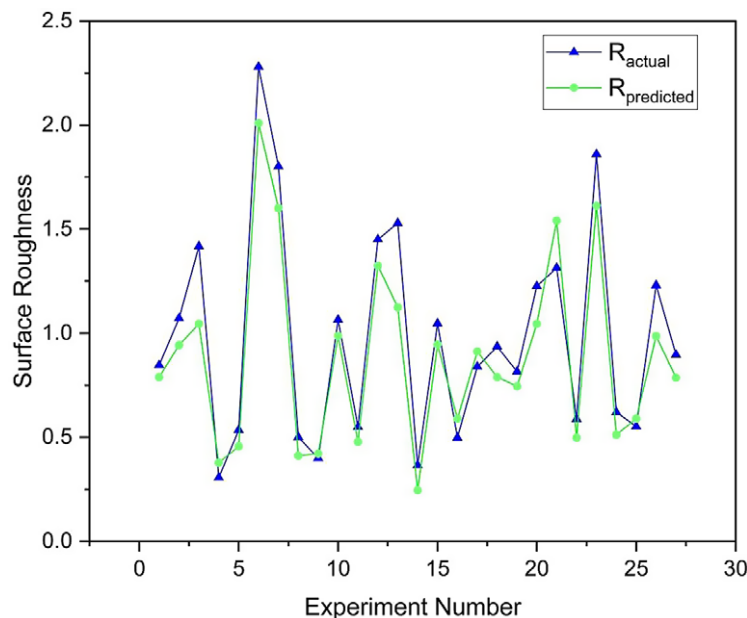


**Figure 7.** Measured surface roughness ( $R_{actual}$ ) vs predicted surface roughness ( $R_{predict}$ ) for model 2.

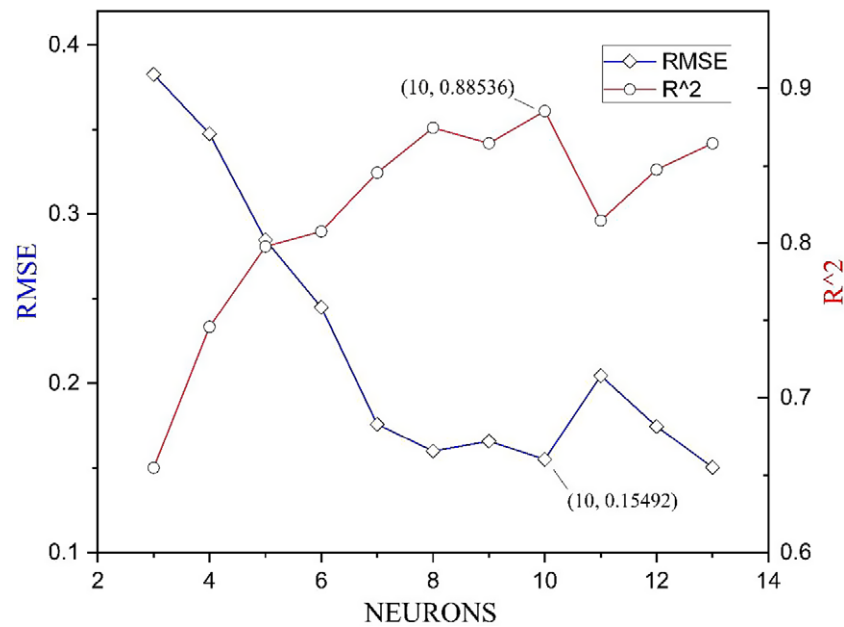


**Figure 8.** Calculated RMSE and  $R^2$  values at each hidden neuron for model 2.

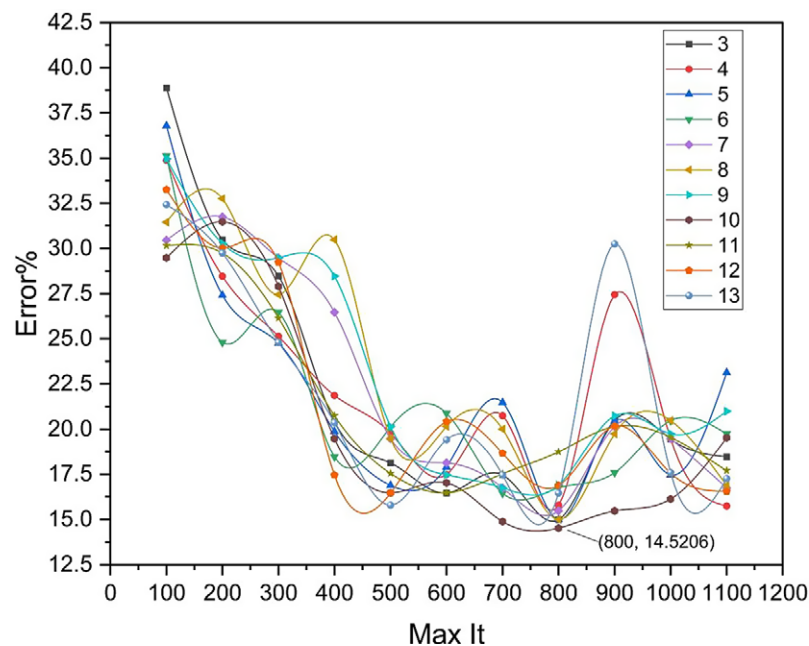


**Figure 9.** Calculated error percentage at each maximum iteration and each hidden neuron for model 2.

### Sound characteristics based hybrid model

This section discusses the performance studies of TLBO-trained ANN structure for sound characteristics. This hybrid neural network provides optimized weights and biases, which are able to reduce the error function in a short span of time. These weights and biases are consecutively changing until they reach the convergence criterion. As discussed in earlier sections, the optimized ANN structure is obtained by changing controlling factors such as the number of hidden neurons, population size, and number of iterations. A smaller population size may lead to convergence

towards the global solution, whereas a larger population size takes more time to converge the solution.

The sensitivity test has been performed for a sound characteristics-based hybrid model to find the optimal value of population size. This sensitivity test was performed on various population sizes ranging from 25 to 275 with a step size of 25. From Figure 10, it is noticed that the ANN-TLBO algorithm gives better results and takes more time to converge the solution, and more iterations are needed when running at a smaller population size.



**Table 6.** Model-2 RMSE and  $R^2$  values for different neurons generated by the algorithm.

Neuron	RMSE	$R^2$
3	0.382	0.654
4	0.347	0.745
5	0.284	0.797
6	0.245	0.807
7	0.175	0.845
8	0.159	0.874
9	0.165	0.864
10	0.154	0.885
11	0.204	0.814
12	0.174	0.847
13	0.150	0.864

The global best optimum is achieved at a population size of 125 with minimum computational cost. In the same way, a sensitivity test was conducted for different numbers of iterations at the obtained optimal population size of 125. This sensitivity test also reveals that the MSE value decreases with an increase in the number of iterations. The test has been performed with various iteration numbers ranging from 100 to 1100 with step size 100. As Figure 12 shows the iteration number of 700 is chosen as another optimal parameter for ANN-TLBO structure. Afterward, there is no massive difference observed in MSE when iteration increases from the optimal value. The RMSE, correlation coefficient ( $R^2$ ), and MEP values obtained with these algorithms are shown in Tables 8 and 9.

**Result**

Hybrid model validation: The hybrid neural network optimizes weights through techniques like GA, PSO, ant colony, and BAT, requiring sensitivity analysis by adjusting parameters, including

**Table 7.** Model-2 MEP values for different neurons generated by the algorithm.

Max It	3	4	5	6	7	8	9	10	11	12	13
100	38.876	34.874	36.784	35.126	30.457	31.451	34.964	29.475	30.152	33.256	32.415
200	30.47	28.456	27.412	24.789	31.745	32.745	30.265	31.475	29.745	30.014	29.745
300	28.475	25.123	24.756	26.475	29.475	27.451	29.475	27.897	26.147	29.235	24.789
400	20.415	21.867	19.874	18.457	26.475	30.478	28.47	19.475	20.741	17.451	20.364
500	18.125	19.784	16.879	20.123	19.475	19.475	20.14	16.472	17.54	16.457	15.784
600	16.452	17.487	17.897	20.879	18.124	20.145	17.456	17.021	16.47	20.417	19.415
700	17.456	20.745	21.476	16.451	16.745	20.007	16.748	14.889	17.523	18.654	17.451
800	14.987	15.784	14.997	16.745	15.478	15.004	16.897	14.5206	18.741	16.874	16.457
900	20.475	27.451	20.457	17.587	20.147	19.745	20.745	15.475	20.147	20.178	30.241
1000	19.456	19.475	17.456	20.475	19.475	20.478	19.745	16.124	19.542	17.562	17.584
1100	18.457	15.745	23.126	19.745	16.745	16.874	20.987	19.526	17.697	16.547	17.254

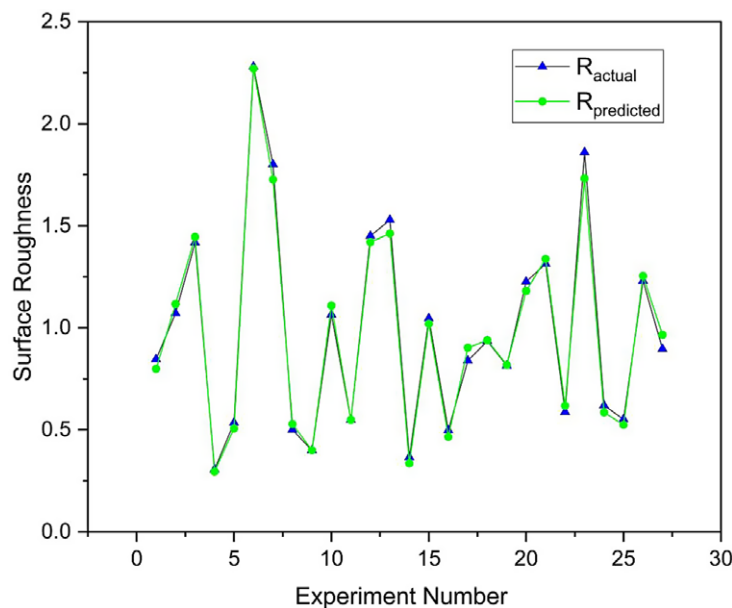


**Figure 10.** Measured surface roughness ( $R_{actual}$ ) vs predicted surface roughness ( $R_{predict}$ ) for model 3.

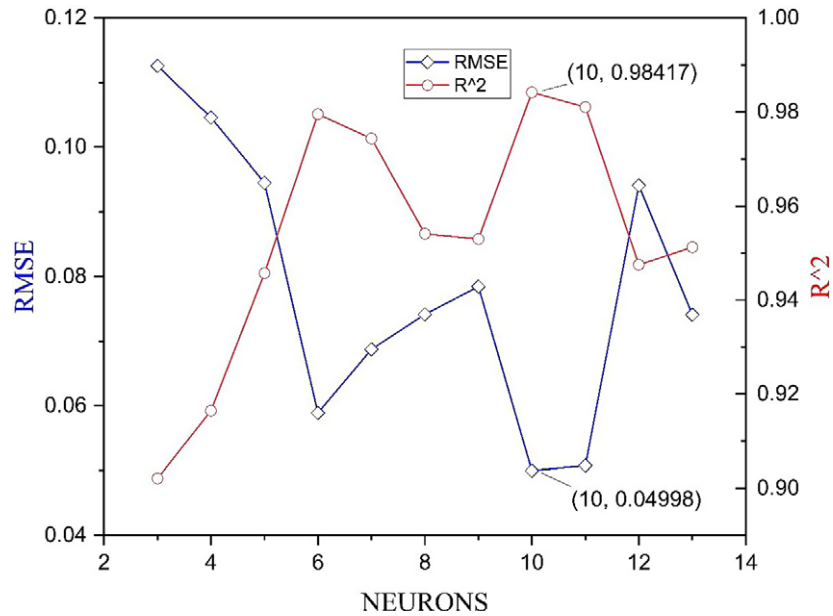


Figure 11. Calculated RMSE and  $R^2$  values at each hidden neuron for model 3.

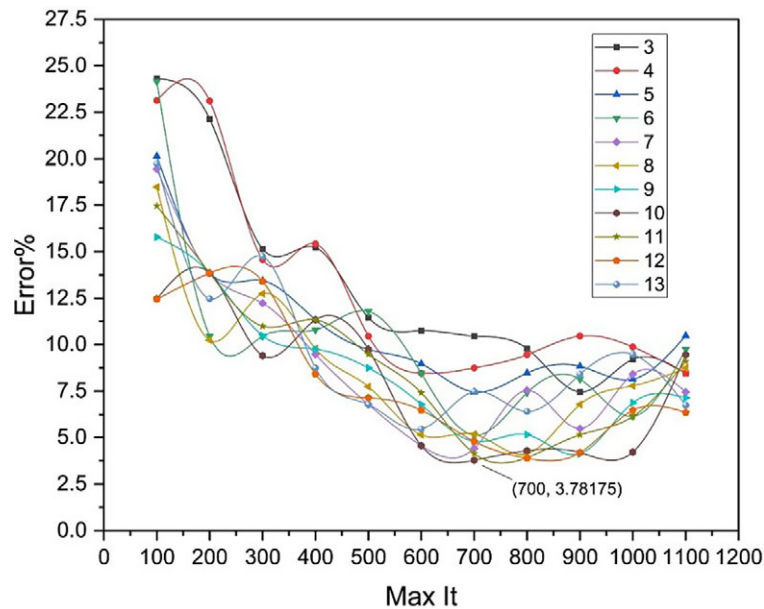


Figure 12. Calculated error percentage at each maximum iteration and each hidden neuron for model 3.

population size, crossover rate, mutation rate, and criteria. To reduce the computational load, the TLBO algorithm is fine-tuned for enhanced performance with reduced sensitivity to parameters, ultimately achieving superior efficiency and performance as mentioned by (Togan, 2012). Examining the impact of machining parameters (MPs) on vibration signals (VS), and surface roughness (SR) in aluminum alloy CNC machining, the ANN models show outstanding correlation factors ( $R$  values 0.97–1), providing insights for improving CNC machining efficiency. A sensitivity analysis fine-tunes the optimal hybrid neural network, linking performance to hidden layer configuration, and neuron count, with the neural independence test revealing optimal counts of

6 and 10 hidden neurons for model 1 and the remaining models, respectively.

The sensitivity analysis: The developed hybrid models (i.e., models 1, 2, and 3), the error percentages for each model are depicted in Figure 13. Examining the graph presented in Figure 13, it becomes evident that the vibration-based model exhibits a relatively high error rate, approaching 33%, with an average error of approximately 14.520 when predicting surface roughness. Conversely, the cutting parameters-based model displays a more modest average error percentage of 4.746. However, the standout performer is the sound-based surface roughness model, boasting an impressive average error rate of 3.76. This

**Table 8.** Model-3 RMSE and  $R^2$  values for different neurons generated by the algorithm

Neuron	RMSE	$R^2$
3	0.112	0.902
4	0.104	0.916
5	0.094	0.945
6	0.058	0.979
7	0.068	0.974
8	0.074	0.954
9	0.078	0.953
10	0.049	0.984
11	0.050	0.981
12	0.094	0.947
13	0.074	0.951

compellingly demonstrates that the sound-based model outperforms the other two models in terms of its predictive accuracy for surface roughness.

Comparison with recent literature: nevertheless, the performance assessment of the developed sound-based hybrid model is compared to recent studies and is listed in Table 10. From the studies presented in Table 10, it is evident that the newly developed sound-based hybrid neural network outperforms the others, achieving an impressive accuracy rate of 96%. This finding underscores the effectiveness of our sound-based hybrid neural network for accurately predicting surface roughness in face-milled components.

The sound measurements and model-3 outperform vibrations and cutting parameters. Numerous studies have demonstrated the efficacy of sound measures for detecting bearing defects, showcasing their ability to identify flaws before they manifest as visible vibrations post-failure (Tandon and Choudhury, 1999). The sensitivity of sound measurements, capturing high-frequency data, enables early defect detection by extracting modulations correlated to machine fault frequencies. The study based on sound measurements can

**Table 9.** Model-3 MEP values for different neurons generated by the algorithm.

Max It	3	4	5	6	7	8	9	10	11	12	13
100	24.31	23.124	20.14	24.14	19.45	18.475	15.784	12.47	17.45	12.45	19.745
200	22.14	23.102	13.85	10.45	13.85	10.235	13.85	13.85	13.85	13.85	12.475
300	15.14	14.578	13.45	10.45	12.235	12.745	10.475	9.41	10.98	13.41	14.752
400	15.23	15.42	11.33	10.784	9.475	9.784	9.748	11.33	11.33	8.412	8.745
500	11.45	10.45	9.74	11.78	6.784	7.741	8.745	9.745	9.475	7.1452	6.784
600	10.74	8.457	8.974	8.456	4.56	5.142	6.784	4.56	7.415	6.478	5.452
700	10.457	8.745	7.456	5.124	4.412	5.174	4.789	3.781	4.134	4.785	7.478
800	9.78	9.451	8.472	7.415	7.546	4.125	5.147	4.287	3.925	3.885	6.415
900	7.46	10.462	8.841	8.142	5.475	6.784	4.123	4.189	5.147	4.189	8.41
1000	9.214	9.874	8.142	6.145	8.41	7.789	6.879	4.214	6.142	6.475	9.475
1100	8.451	8.457	10.475	9.745	7.457	8.7456	7.145	9.452	9.1	6.358	6.745

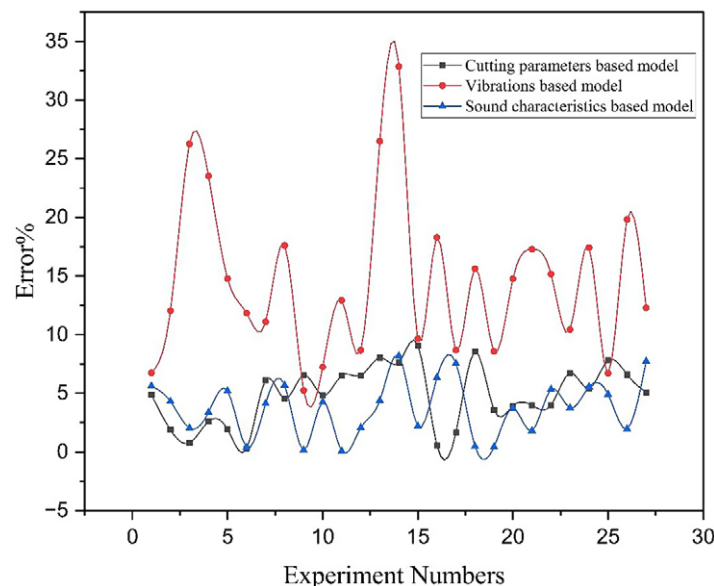


**Figure 13.** Comparison of developed models.

**Table 10.** Model comparison with recent literature.

S. no	Process	Model	Description	References
1.	CNC milling process	FFT–LSTM	An FFT–LSTM model predicts surface roughness values using vibration signals as input, achieving a MAPE of 23.5%.	Lin <i>et al.</i> (2019)
2.	CNC turning process	Firefly–LSTM	A Firefly–LSTM model predicts surface roughness values using machining process vibration signals, achieving an RMSE of 0.248.	Andrews <i>et al.</i> (2023)
3.	CNC milling process	PSO–LSSVM	The model predicts surface roughness with accuracy (92.54%) using input data from noise, vibration, and workpiece surface texture characteristics.	Li <i>et al.</i> (2022)
4.	Grinding process	PSO–LS–SVR	The model predicts surface roughness with accuracy of (92%) using input data from noise characteristics.	Nguyen <i>et al.</i> (2022)
5.	End milling process	Deep learning neural networks	The model accurately predicts surface roughness with accuracy of (90%) using noise characteristics data.	Bhandari <i>et al.</i> (2023)
6.	Hard Turning process	Fuzzy logic model	This model predicts surface roughness with accuracy of (86%) using input data from vibration and acoustic emissions.	Asiltürk <i>et al.</i> (2023)
7.	CNC milling process	One dimensional convolutional neural network (1D–CNN)	This model predicts surface roughness with accuracy of (94.56%) using input data solely from vibration.	Zeng <i>et al.</i> (2023)
8.	End milling process	One dimensional convolutional neural network (1D–CNN) with Mel-Spectrogram	This model predicts surface roughness accurately with accuracy of (90%) using input data from sound and force datasets.	Bhandari (2021)
9.	CNC milling process	ANN–TLBO	This model takes input data from sound data set, and successfully predicts surface roughness, achieving a high prediction accuracy of 96.218 % and having the RMSE of 0.04998.	Present work

detect minute fluctuations and micro-level surface noise, and suggest potential enhancements in roughness assessment prediction skills.

### IoT interface/mobile interface

ANN–TLBO is used to develop a model for surface roughness prediction. Each neuron's weights and biases are collected, and using those values, an equation for surface roughness is developed. The mobile app described in the paper is not directly functioning as a traditional IoT system in terms of machine-to-mobile data transfer. However, the purpose of the mobile app is to serve as an interface for open architectural machine tools. With the availability of open-architecture machine tools, one can seamlessly integrate this mobile interface into the systems, effectively serving as an IoT bridge between the machine and the mobile app. By interfacing with such machines, it becomes possible to establish a direct channel for data transfer from the machine to the mobile device. In this way, the mobile app facilitates the interaction between the user and the machine, allowing real-time data sharing and control. The mobile application is developed using FLUTTER software, which acts as a creative maestro conducting a pixel symphony. It expertly fuses the art of design with the science of coding, enabling developers to build visually appealing and engaging user experiences. Due to its adaptable performance and cross-platform capabilities, Flutter bounces across platforms like a digital chameleon, easily merging with smartphones, tablets, web browsers, and more. It supports the spirit of flexibility and provides developers with the ability to let their imaginations run wild and gracefully and skilfully accomplish their software

objectives. The developed mobile interface has text fields for input and output that can be filled out manually. The roughness is calculated using the surface roughness equation based on the user's inputs, and the result values are displayed on the mobile interface. One of the numerous advantages of this approach is that it provides a user-friendly interface that can be used to rapidly and easily predict surface roughness for a given set of input data. An ANN–TLBO algorithm can effectively and accurately predict surface roughness, and the mobile interface makes it simple to access and utilize the model from a mobile device. Overall, in a wide range of industries, including manufacturing and engineering, the ability to predict surface roughness is essential for achieving the highest possible product quality and performance. The prediction model has become more accessible and simpler to use because of the development of a mobile interface, making it a useful tool for field engineers and technicians.

In order to predict and display the surface roughness online used the flutter platform. An equation derived to predict the surface roughness from the ANN–TLBO hybrid model based on the weights and bias is shown below in Eq. (15). Where  $S_1$  is mean,  $S_2$  is standard deviation,  $S_3$  is Skewness, and  $S_4$  is Kurtosis values of sound characteristic.

$$R_a = (-0.5108H_1) + (0.3146H_2) + (0.003H_3) + (0.5858H_4) + (1.6860H_5) + (0.8526H_6) - (1.5632H_7) - (0.5600H_8) + (0.5189H_9) + (0.3066H_{10}) + 0.8789 \quad (15)$$

where  $H_1$  to  $H_{10}$  are calculated using the following Eqs. (16)–(26).



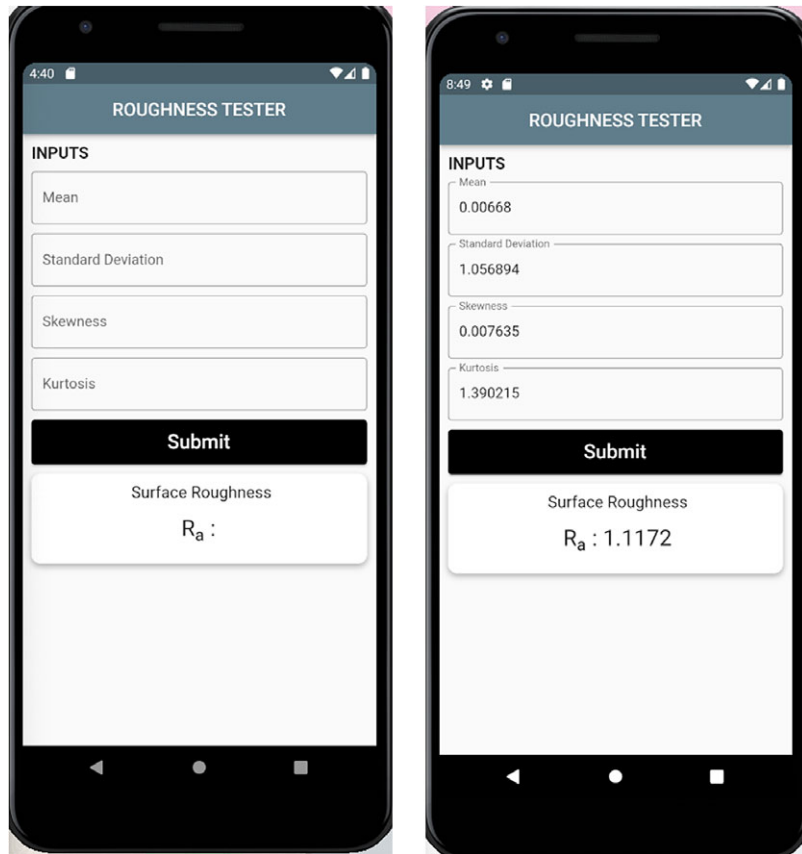


Figure 14. (a) Mobile app input interface and (b) Mobile app output Interface.

$$H1 = \frac{1}{1 + e^{-(0.9551*S1 - 2.1782*S2 - 0.3310*S3 - 4.9999*S4 - 0.5108)}} \quad (16)$$

$$H2 = \frac{1}{1 + e^{-( -5*S1 + 2.3421*S2 - 4.9999*S3 - 2.5533*S4 + 0.3146)}} \quad (17)$$

$$H3 = \frac{1}{1 + e^{-(0.5577*S1 + 4.920*S2 - 4.9209*S3 - 3.0732*S4 + 0.0032)}} \quad (18)$$

$$H4 = \frac{1}{1 + e^{-( -5*S1 - 0.1591*S2 + 2.7145*S3 - 0.0160*S4 + 0.5858)}} \quad (20)$$

$$H5 = \frac{1}{1 + e^{-( -2.2334*S1 - 0.4782*S2 - 2.8161*S3 - 4.980854*S4 + 1.6860)}} \quad (21)$$

$$H6 = \frac{1}{1 + e^{-(4.9975*S1 - 1.752052*S2 + 0.2447*S3 - 2.6833*S4 + 0.8526)}} \quad (22)$$

$$H7 = \frac{1}{1 + e^{-(1.25625*S1 - 1.752052*S2 + 0.2447*S3 - 2.683354*S4 + 0.8526)}} \quad (23)$$

$$H8 = \frac{1}{1 + e^{-(2.5357*S1 - 0.8974*S2 - 0.1521*S3 + 0.7055*S4 - 0.5600)}} \quad (24)$$

$$H9 = \frac{1}{1 + e^{-( -0.1140*S1 - 2.880852*S2 - 3.2729*S3 - 2.719754*S4 + 0.5189)}} \quad (25)$$

$$H10 = \frac{1}{1 + e^{-( -0.5461*S1 + 4.9912*S2 - 0.2006*S3 + 3.0732*S4 + 0.3066)}} \quad (26)$$

From the earlier discussion, it is clearly identified that the sound characteristic data-based hybrid neural network (i.e., model 3) shows better performance as compared to other developed models 1 and 2. So, the authors developed the mobile app interface for model 3 as shown in Figure 14. The sound characteristic data of the machined samples are given as input data for the developed mobile app input interface (Figure 14a). The application performance results after entering input data and model predicted values are displayed in the output interface as shown in Figure 14b. Therefore, the developed mobile app interface reduces the cost and labor effort and is effectively used to predict the surface roughness of the machined samples.

### Conclusion

This study, developed and analyzed three hybrid models aimed at forecasting surface roughness during the machining process. Leveraging ANN in combination with TLBO, these models consider cutting parameters, vibration data, and sound characteristics as crucial input elements.

- Key findings and optimization parameters:

Model-1: Cutting parameters-based model for surface roughness prediction. the architecture is designed with six hidden neurons ( $H_o$ ), a population size ( $n_{pop}$ ) of 125, and a Max It of 700. Model-2: vibration-based model for surface roughness prediction. the architecture is designed with 10 hidden neurons ( $H_o$ ), a population size ( $n_{pop}$ ) of 200, and a Max It of 800. Model-3: sound characteristics-based model for surface roughness prediction. the architecture is designed with 10 hidden neurons ( $H_o$ ), a population size ( $n_{pop}$ ) of 125, and a maximum iteration (Max It) of 1100.

- Model evaluation and comparison:

Training set of 26 points and a separate test set of one point created using “Leave-One-Out Cross-Validation” (LOOCV). Model performance metrics reveal excellent accuracy: Model 1 (cutting parameters) with RMSE 0.068, R2 0.9931; Model 2 (vibrations) with RMSE 0.15492, R2 0.88536; Model 3 (sound characteristics) excelling at RMSE 0.04998, R<sup>2</sup> 0.98417. The model considered the best is the one with an R<sup>2</sup> close to 1 and an RMSE close to 0. In this instance, Model 3 demonstrated superior results compared to the other two models.

- Models percentage error analysis and superiority:

Sound-based Model 3 demonstrated exceptional accuracy (average error percentage: 3.77%), outperforming Model 2 (14.52%) and Model 1 (4.75%). Comparative analysis with recent studies showcased an impressive 96% accuracy for the sound-based hybrid model, establishing its superiority.

- IoT mobile interface development:

An IoT mobile interface using the flutter platform was developed for practical usability. Users can input sound characteristics and receive real-time predictions of surface roughness. Catering to field engineers and technicians, the interface enhances accessibility and usability.

This study validates the effectiveness of hybrid ANN–TLBO models for accurate surface roughness prediction in machining processes. The sound-based model, in particular, emerges as a promising tool for various industrial applications. The development of a user-friendly mobile interface enhances the accessibility and usability of these predictive models, making them valuable assets in the field of manufacturing and engineering.

### Future scope of work

In our upcoming work, we intend to broaden the model’s applicability to include a larger range of cutting circumstances, including various machining procedures and cutting instruments. We seek to increase the model’s adaptability by performing in-depth research and validation trials, making it suitable for a number of circumstances frequently seen in machining operations. In order to provide insightful analysis and precise surface roughness forecasts in a variety of industrial scenarios, we are eager to investigate the possibilities of our model in various cutting circumstances and processes.

**Supplementary material.** The supplementary material for this article can be found at <http://doi.org/10.1017/S0890060424000192>.

### References

- Abbas AT, Pimenov DY, Erdakov IN, Mikolajczyk T, Soliman MS and El Rayes MM (2019) Optimization of cutting conditions using artificial neural networks and the Edgeworth–Pareto method for CNC face-milling operations on high-strength grade-H steel. *The International Journal of Advanced Manufacturing Technology*, **105**, 2151–2165. <https://doi.org/10.1007/s00170-019-04327-4>
- Anagün Y, Işık Ş and Çakır F H (2023) Surface roughness classification of electro discharge machined surfaces with deep ensemble learning. *Measurement* **215**, 112855. <https://doi.org/10.1016/j.measurement.2023.112855>
- Andrews A, Manisekar K and Rex MT (2023) An expert system for vibration-based surface roughness prediction using firefly algorithm and LSTM network. *Journal of the Brazilian Society of Mechanical Sciences and Engineering* **45**, 414. <https://doi.org/10.1007/s40430-023-04341-4>
- Asiltürk İ, Kuntoglu M, Binali R, Akkuş H and Salur E (2023) A comprehensive analysis of surface roughness, vibration, and acoustic emissions based on machine learning during hard turning of AISI 4140 steel. *Metals* **13**(2), 437. <https://doi.org/10.3390/met13020437>
- Balasubramanian KR, Ravi Kumar K, Sathiyaa Prabhakaran SP, Jinshah BS and Abhishek N (2022) Thermal degradation studies and hybrid neural network modelling of eutectic phase change material composites. *International Journal of Energy Research*. **46**(11), 15733–15755. <https://doi.org/10.1002/er.8272>
- Bhandari B (2021) Comparative study of popular deep learning models for machining roughness classification using sound and force signals. *Micro-machines*, **12**(12), 1484. <https://doi.org/10.3390/mi12121484>
- Bhandari B, Park G, & Shafiabady N (2023). Implementation of transformer-based deep learning architecture for the development of surface roughness classifier using sound and cutting force signals. *Neural Computing and Applications*, **35**(18), 13275–13292. <https://doi.org/10.1007/s00521-023-08425-z>
- Bhowmick S, Mondal R, Sarkar S, Biswas N, De J, Majumdar G (2023) Parametric optimization and prediction of MRR and surface roughness of titanium mixed EDM for Inconel 718 using RSM and fuzzy logic. *CIRP Journal of Manufacturing Science and Technology*. **40**, 10–28. <https://doi.org/10.1016/j.cirpj.2022.11.002>
- Buj-Corral I, Sender P, Luis-Pérez CJ (2023) Modeling of surface roughness in Honing processes by using fuzzy artificial neural networks. *Journal of Manufacturing and Materials Processing*. **7**(1), 23. <https://doi.org/10.3390/jmmp7010023>
- Chebrolu V, Koona R, Raju RS (2022) Automated evaluation of surface roughness using machine vision based intelligent systems. *Journal of Scientific & Industrial Research*. **82**(1), 11–25. <http://op.niscpr.res.in/index.php/JSIR/article/view/69946>
- Eser, A, Aşkar Ayyıldız, E, Ayyıldız, M and Kara, F (2021) Artificial intelligence-based surface roughness estimation modelling for milling of AA6061 alloy. *Advances in Materials Science and Engineering* **2021**, 1–10. <https://doi.org/10.1155/2021/5576600>
- Feng Y, Hsu FC, Lu YT, Lin YF, Lin CT, Lin CF, Lu YC, Lu X, Liang SY (2020) Surface roughness prediction in ultrasonic vibration-assisted milling. *Journal of Advanced Mechanical Design, Systems, and Manufacturing*. **14**(4), JAMDSM0063. <https://doi.org/10.1299/jamdsm.2020jamdsm0063>
- Guleria V, Kumar V and Singh PK (2022) Prediction of surface roughness in turning using vibration features selected by largest Lyapunov exponent based ICEEMDAN decomposition. *Measurement* **202**, 111812. <https://doi.org/10.1016/j.measurement.2022.111812>
- Ho WH, Tsai JT, Lin BT, Chou JH (2009) Adaptive network-based fuzzy inference system for prediction of surface roughness in end milling process using hybrid Taguchi-genetic learning algorithm. *Expert Systems with Applications* **36**(2), 3216–3222. <https://doi.org/10.1016/j.eswa.2008.01.051>
- Hornás, J, Běhal, J, Homola, P, Senck, S, Holzleitner, M, Godja, N, Pásztor, Z, Hegedüs, B, Doubrava, R, Růžek, R and Petrusová, L (2023) Modelling fatigue life prediction of additively manufactured Ti-6Al-4V samples using machine learning approach. *International Journal of Fatigue*, **169**:107483. <https://doi.org/10.1016/j.ijfatigue.2022.107483>
- Huang, PB, Inderawati, MMW, Rohmat, R (2023) The development of an ANN surface roughness prediction system of multiple materials in turning. *The International Journal of Advanced Manufacturing Technology* **125**, 1193–1211. <https://doi.org/10.1007/s00170-022-10709-y>
- Kara, F, Bulan, N, Akgün, M and Köklü, U (2023) Multi-objective optimization of process parameters in milling of 17-4 PH stainless steel using taguchi-based gray relational analysis. *Engineered Science*, **26**, 961. <https://doi.org/10.30919/es961>
- Kara, F, Karabatak, M, Ayyıldız, M and Nas, E (2020) Effect of machinability, microstructure and hardness of deep cryogenic treatment in hard turning of AISI D2 steel with ceramic cutting. *Journal of Materials Research and Technology*, **9**(1), 969–983. <https://doi.org/10.1016/j.jmrt.2019.11.037>
- Kottala RK, Chigilipalli BK, Mukuloth S, Shanmugam R, Kantumuchu VC, Ainapurapu SB, Cheepu M (2023) Thermal degradation studies and machine learning modelling of nano-enhanced sugar alcohol-based phase change materials for medium temperature applications. *Energies*. **16**(5), 2187. <https://doi.org/10.3390/en16052187>

- Kottala RK, Ramaraj BK, BS J, Vempally MG, Lakshmanan M** (2022) Experimental investigation and neural network modeling of binary eutectic/expanded graphite composites for medium temperature thermal energy storage. *Energy Sources, Part A: Recovery, Utilization, and Environmental Effects*, 1–24. <https://doi.org/10.1080/15567036.2022.2043490>
- Kumar KR, Balasubramanian KR, Kumar GP, Bharat Kumar C, Cheepu MM** (2022) Experimental investigation of nano-encapsulated molten salt for medium-temperature thermal storage systems and modeling of neural networks. *International Journal of Thermophysics*, 43(9), 145. <https://doi.org/10.1007/s10765-022-03069-y>
- Kundu, P, Luo, X, Qin, Y, Cai, Y and Liu, Z** (2022) A machine learning-based framework for automatic identification of process and product fingerprints for smart manufacturing systems. *Journal of Manufacturing Processes*, 73, 128138. <https://doi.org/10.1016/j.jmapro.2021.10.060>
- Li S, Li S., Liu Z, & Vladimirovich, PA** (2022) Roughness prediction model of milling noise-vibration-surface texture multi-dimensional feature fusion for N6 nickel metal. *Journal of Manufacturing Processes*, 79, 166–176. <https://doi.org/10.1016/j.jmapro.2022.04.055>
- Lin WJ, Lo SH, Young HT and Hung CL** (2019) Evaluation of deep learning neural networks for surface roughness prediction using vibration signal analysis. *Applied Sciences*, 9(7), 1462. <https://doi.org/10.3390/app9071462>
- Mikolajczyk T and Olaru A** (2015) Some methods of research results approximation. *Applied Mechanics and Materials*, 783, 95–103. <https://doi.org/10.4028/www.scientific.net/amm.783.95>
- Mikolajczyk T** (2014) Modeling of minimal thickness cutting layer influence on surface roughness in turning. *Applied Mechanics and Materials*, 656, 262–269. <https://doi.org/10.4028/www.scientific.net/AMM.656.262>
- Mikolajczyk T, Fuwen H, Moldovan L, Bustillo A, Matuszewski M and Nowicki K** (2018) Selection of machining parameters with Android application made using MIT App Inventor bookmarks. *Procedia Manufacturing*, 22, 172–179. <https://doi.org/10.1016/j.promfg.2018.03.027>
- Mikolajczyk T, Latos H, Pimenov DY, Paczkowski T, Gupta MK and Krolczyk G** (2020) Influence of the main cutting edge angle value on minimum uncut chip thickness during turning of C45 steel. *Journal of Manufacturing Processes*, 57, 354–362. <https://doi.org/10.1016/j.jmapro.2020.06.040>
- Nguyen VH, Vuong TH, and Nguyen QT** (2022) Feature representation of audible sound signal in monitoring surface roughness of the grinding process. *Production & Manufacturing Research*, 10(1), 606–623. <https://doi.org/10.1080/21693277.2022.2108927>
- Raju RU, Raju VR, Ramesh R** (2017) Curvelet transform for estimation of machining performance. *Optik* 131, 615–625. <https://doi.org/10.1016/j.ijleo.2016.11.181>
- Rao RV, Savsani VJ, Vakharia DP** (2012) Teaching–learning-based optimization: an optimization method for continuous non-linear large scale problems. *Information sciences*, 15;183(1), 1–5. <https://doi.org/10.1016/j.ins.2011.08.006>
- RS UR, Ramesh R and Rohit Varma K** (2020) Development of surface texture evaluation system for highly sparse data-driven machining domains. *International Journal of Computer Integrated Manufacturing*, 33(9), 859–868. <https://doi.org/10.1080/0951192X.2020.1803503>
- Salgado DR, Cambero I, Marcelo A and Alonso FJ** (2009) Surface roughness prediction based on the correlation between surface roughness and cutting vibrations in dry turning with TiN-coated carbide tools. *Proceedings of the Institution of Mechanical Engineers, Part B: Journal of Engineering Manufacture*, 223(9), 1193–1205. <https://doi.org/10.1243/09544054JEM1508>
- Singh SK, Srinivasan K, Chakraborty D** (2004) Acoustic characterization and prediction of surface roughness. *Journal of Materials Processing Technology*, 152(2), 127–130. <https://doi.org/10.1016/j.jmatprotec.2004.03.023>
- Tandon N and Choudhury A** (1999) A review of vibration and acoustic measurement methods for the detection of defects in rolling element bearings. *Tribology International*, 32(8), 469–480. [https://doi.org/10.1016/S0301-679X\(99\)00077-8](https://doi.org/10.1016/S0301-679X(99)00077-8)
- Togan V** (2012) Design of planar steel frames using teaching-learning based optimization. *Engineering Structures* 34, 225–234. <https://doi.org/10.1016/j.engstruct.2011.08.035>
- Tseng TL, Konada U, Kwon Y** (2016) A novel approach to predict surface roughness in machining operations using fuzzy set theory. *Journal of Computational Design and Engineering*, 3(1), 1–3. <https://doi.org/10.1016/j.jcde.2015.04.002>
- Wu TY, Lei KW** (2019) Prediction of surface roughness in milling process using vibration signal analysis and artificial neural network. *The International Journal of Advanced Manufacturing Technology*, 102(1-4), 305–314. <https://doi.org/10.1007/s00170-018-3176-2>
- Yücel Y, Otuzbir Ö, Yücel E** (2023) Surface roughness prediction in SILAR coating process of ZnO thin films: mathematical modelling and validation. *Materials Today Communications*, 1;34, 105101. <https://doi.org/10.1016/j.mtcomm.2022.105101>
- Zeng S, Pi D, and Xu, T** (2023). Milling surface roughness prediction method based on spatiotemporal ensemble learning. *The International Journal of Advanced Manufacturing Technology*, 1–29. <https://doi.org/10.1007/s00170-023-11737-y>
- Zhao Z, Wang S, Wang Z, Wang S, Ma C, Yang B** (2022) Surface roughness stabilization method based on digital twin-driven machining parameters self-adaptation adjustment: a case study in five-axis machining. *Journal of Intelligent Manufacturing*, 1–10. <https://doi.org/10.1007/s10845-020-01698-4>
- Župerl U and Čuš F** (2019) A cyber-physical system for surface roughness monitoring in end-milling. *Journal of Mechanical Engineering/Strojniški Vestnik*, 65(2). <https://doi:10.5545/sv-jme.2018.5792>

**Author biographies.** Dr. R S Umamaheswara Raju is an Associate Professor in the Department of Mechanical engineering at The M V G R College of Engineering (A), Vizianagaram, AP, India. Perused his Ph.D. from JNTUK, Kakinada, Andhra Pradesh, India in development of performance-based enhancement systems for open architectural controlled CNC machine tools. Published his work in 15 peer reviewed journals, published 2 patents, and attended several conferences.

Dr. Ravi Kumar Kottala is an assistant professor at M V G R College of Engineering (A), Vizianagaram, specializing in ANSYS Workbench, APDL, Creo 2.0, MATLAB Simulink, and various mechanical and manufacturing concepts. He is proficient in Microsoft Word, Python, battery thermal management, Solar PV installation, leadership, and Blender. Dr. Kottala holds a postgraduate degree from the National Institute of Technology Tiruchirappalli and completed his Ph.D. from the same institution. He has authored several international journals in his field.

Dr. B Madhava Varma is an Associate Professor in the Department of Mechanical Engineering at Maharaj Vijayaram Gajapathiraj College of Engineering, located in Chintalavalasa, Vizianagaram, Andhra Pradesh, India. He holds a Ph. D. degree from JNTUA Ananthapuramu, Andhra Pradesh, India. His research interests primarily focus on investigating the effects of alternate fuels on various aspects of Internal Combustion Engines (IC Engines), including vibration, noise, combustion, and performance. Additionally, he is involved in research related to the condition monitoring of machines and engines. He has successfully completed a minor research project funded by the University Grants Commission (UGC) in New Delhi, India. The project focused on engine vibration analysis utilizing biofuels. This indicates his commitment to exploring sustainable and alternative energy sources for engines while addressing environmental concerns.

Mr. Palla Krishna is a student in the Department of mechanical engineering (2020-23) at the MVGR College of Engineering (A), Vizianagaram, AP, India. Perused many certificate courses on Artificial intelligence, machine learning, Manufacturing technology and Origin pro. Working on the projects under the guidance of Dr. R S Umamaheswara Raju.

Dr. Praveen Barmavatu currently serves as an assistant professor at the Department of Mechanical Engineering, Faculty of Engineering, Universidad Tecnológica Metropolitana, located at Av. José Pedro Alessandri 1242, Santiago, Chile. He completed his Diploma at Government Polytechnic College and obtained his B.Tech and M.Tech degrees from JNTU. Additionally, he earned a Doctor of Philosophy degree from Shri JNT University. Dr. Barmavatu has contributed significantly to research, with publications in various international journals and patents to his credit.